Letters

Improving High-Frequency Performance of an Input Common Mode EMI Filter Using an Impedance-Mismatching Filter

Fang Luo, Dong Dong, Dushan Boroyevich, Paolo Mattavelli, and Shuo Wang

***Abstract*—This letter investigates into the impedance interaction between the electromagnetic interference (EMI) filter and the noise propagation path, and its influences on the filter design. It proves that the impedance resonance in the propagation path decreases the filter's high-frequency in-circuit attenuation. This letter proposes a method to improve the filter's high-frequency performance using an impedance-mismatching filter. The impedance-mismatching filter damps the resonance in the common mode (CM) noise propagation path and eliminates the high-frequency noise spike. By applying this method in the filter design, the CM inductor of the EMI filter can be significantly reduced since the EMI filter avoids the overdesign caused by its high-frequency performance degradation, and the filter can potentially achieve high power density. This letter also proposed a design procedure for this impedance-mismatching filter. An improved EMI filter design method considering this impedance mismatching is also proposed in this letter.**

***Index Terms*—Common mode filter, electromagnetic interference, impedance mismatching.**

I. Introduction

THE switching converter brings the benefit of efficient power conversion, but it also introduces strong electromagnetic interference (EMI) due to the high-frequency switching. Hence, an EMI filter is a necessary part of the converter system, and it contributes a considerable portion to the volume and weight of the converter [1]. Designers have been struggling for ages trying to reduce this passive part. However, the degradation of the filter's high-frequency performance usually results in a much overdesign of the filter.

The causes of the degradation on the filter's high-frequency performance can be different: the study in [2]–[5] has shown that the parasitics of the filter components, such as the equivalent paralleled capacitor (EPC) on the inductor and the equivalent series inductor of the capacitor, can decrease the filter's attenuation. Appropriate cancellation of these parasitics can help to improve the filter's performance; Shuo *et al.* [4] have pointed out that the mutual coupling between the filter's components and traces can also create unexpected defects in the filter's attenuation, which makes the filter performance deviates from its original design. Putting shielding material and changing the layouts can help to cancel this coupling and improve the filter's performance. Specifically, the study in [5] and [6] has proven that the parasitics from grounding can also decrease the filter's common mode (CM) high-frequency attenuation. Fang *et al.* [7]–[9] have shown that the EMI filter's attenuation is not only determined by the filter's cut-off frequency, but also by the impedance interaction between the filter and noise propagation paths. Specifically, Fang *et al.* [8] report the early finding that using a small filter can effectively eliminate the resonance in the noise spectrum and reduce the size of the main filter. However, how these interactions can influence the filter design stays unclear.

This letter gives a systematic analysis of the impedance interaction and its impacts on the CM filter's high-frequency performance. It starts from a typical "failed" design example which demonstrates the overdesign caused by the filter's high-frequency performance degradation. Then the letter conducts an analysis on this phenomenon using a simplified equivalent circuit and discovers that the filter's degradation in this letter is not caused by the filter's parasitics but by the impedance interaction and resonance in the noise propagation path. Based on this conclusion, the letter proposes a solution to trim this impedance to gain better filter performance using a small impedance-mismatching filter. The last part of the letter shows that the proposed solution effectively improves the filter's attenuation at high frequencies and provides tremendous reduction on the filter's size and weight.

II. Statement of the Problem in an LC EMI Filter

This section introduces the existing problem in a conventional designed EMI filter. In this letter, experiments have been conducted in a 5 kW 300 V dc-fed motor drive system as illustrated in Fig. 1. The motor drive connects with a three-phase motor using a 12-meter-long shielded cable. $L_{\rm cable}$ and $C_{\rm cable}$ are the stray capacitance and inductance of the cable. The chassis of the motor is grounded, thus the motor can also be modeled using the winding-to-chassis capacitance $(C_{\rm s-motor})$ and its winding inductances. $C_{s\rm DC}$ and $C_{s\rm AC}$ are the parasitic capacitances inside the motor drive, which include the capacitance from the layout and the devices. These two stray capacitances usually range from tens to hundreds of picofarad

Manuscript received September 20, 2013; revised January 6, 2014; accepted February 26, 2014. Date of current version May 30, 2014. Recommended for publication by Associate Editor J. Biela.

F. Luo, D. Dong, D. Boroyevich, and P. Mattavelli are with the Department of Electrical and Computer Engineering, Center for Power Electronics Systems, Virginia Tech, Blacksburg, VA 24060 USA (e-mail: fangluo@vt.edu; dongd@vt.edu; dushan@vt.edu; pmatta@vt.edu).

S. Wang is with the Department of Electrical Communication Engineering, University of Texas at San Antonio, San Antonio, TX 78249 USA (e-mail: shuowang@ieee.org).

Color versions of one or more of the figures in this paper are available online at http://ieeexplore.ieee.org.

Digital Object Identifier 10.1109/TPEL.2014.2318038

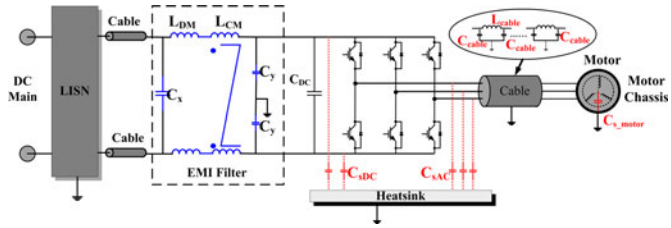

Fig. 1. Motor drive system with an EMI filter.

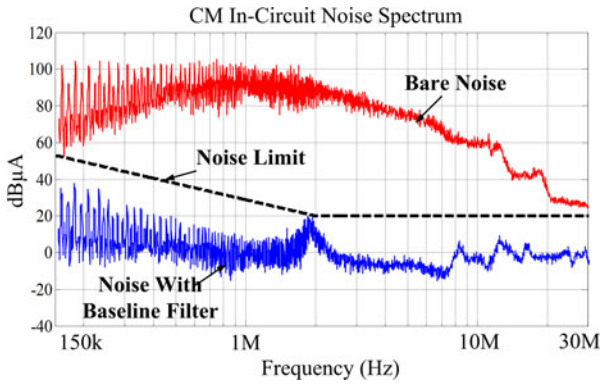

Fig. 2. CM noise current spectrum measurements.

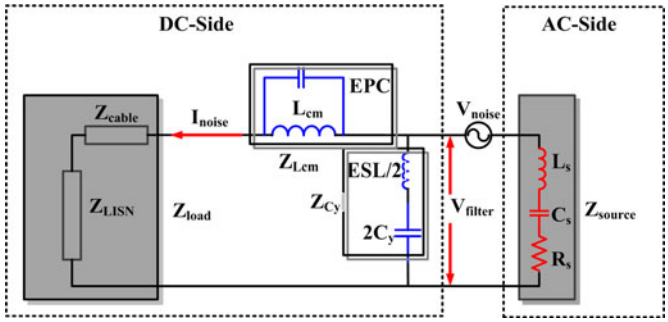

Fig. 3. Equivalent circuit for CM noise propagation path.

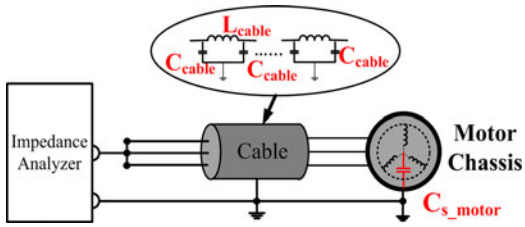

Fig. 4. AC side CM impedance measurement.

in this kind of motor drive. The CM EMI filter capacitor (C_y capacitors) on the dc-side usually ranges from tens up to hundreds of nanofarad, depending on the safety regulation and the power level of the converter. The parasitic capacitances $C_{s\mathrm{DC}}$ and $C_{s\mathrm{AC}}$ can be either extracted using FEA simulation software or measured using the method provided in [8] and [9]. In this letter, $C_{s\mathrm{DC}}$ is 0.8 nF and $C_{s\mathrm{AC}}$ is 45 pF, and C_y is 100 nF per side. The EMI test setup and line-impedance-stabilization network (LISN) in this research is defined by DO-160 standard. The standard also defines the EMI noise current spectrum limit from 150 kHz up to 30 MHz [10]. Following the EMI filter design method proposed in [1], a baseline *LC* EMI filter was designed for this system complying with DO-160 standard limit as shown in Fig. 1.

Fig. 2 illustrates the measured noise current spectrums in this motor drive system. The black-dot-line is the noise limit defined in DO-160. The red curve is the noise without any filters (bare noise) while the blue spectrum is the noise with a typical *LC* EMI filter. Usually the EMI filter is designed according to the low-frequency noise spike amplitude [1]. However, the noise with the baseline *LC* EMI filter in this case shows a resonant spike at 2 MHz, and the attenuation of the filter at this standing-out point does not accommodate with the filter's attenuation designed at low frequencies. Therefore, the filter's parameters need to be overdesigned through error-and-try iterations [1]. In this case, since the total CM capacitance is limited by safety regulation [1], [7], [11], [12], the CM inductor is overdesigned to 3 mH. As shown in Fig. 2, with this baseline filter, the low-frequency and most of the high-frequency noises are over suppressed, but the noise spectrum at 2 MHz is barely touching the noise limit. If this noise spike can be damped properly, the size and weight of the baseline filter should have a chance to get smaller.

III. CM Noise Propagation Path Modeling and Analysis

To understand the cause of the high-frequency noise spike, the motor drive systems shown in Fig. 1 is simplified and modeled with its offline impedances according to [6], [8], [9], [13], [14]. Fig. 3 illustrates the CM equivalent circuit of this system. The noise source can be considered as a voltage source, and its time-domain pattern can be synthesized from the converter's modulation scheme [13]. Z_{cable} represents the impedance of the cable and Z_{LISN} represents the output impedance of the LISN. Z_{source} includes all impedances of the cable and the motor on the ac side. As shown in Fig. 4, Z_{source} can be measured by shorting the ac side line cables and measuring between the lines and the cable shielding (grounding). $C_{s\mathrm{DC}}$ and $C_{s\mathrm{AC}}$ in the motor drive are too small comparing to C_y and the C_{s_motor} so that they can be ignored in the equivalent circuit.

When an *LC* EMI filter is installed on the dc-link, it attenuates the noise current either by shorting the noise current to the ground through C_y capacitor or by blocking the noise current on the power-line using the common-mode inductor L_{cm}. The cutoff frequency f_c of the EMI filter is $f_c = 1/2\pi\sqrt{L_{\mathrm{cm}}C_y}$. When the noise frequency $f >> f_c$, there is $Z_{L\mathrm{cm}} >> Z_{\mathrm{C}y}$, and thus $Z_{\mathrm{C}y}$ is equivalent to the output impedance of the CM filter. Therefore, the $Z_{\mathrm{C}y}$ and the Z_{source} can be considered as a voltage divider for the noise voltage, and the voltage drop V_{filter} on $Z_{\mathrm{C}y}$ becomes the new "noise source" for the following stages, where $V_{\mathrm{filter}} = V_{\mathrm{noise}}Z_{\mathrm{C}y}/(Z_{\mathrm{C}y} + Z_{\mathrm{source}})$, and thus the noise current with filter can be approximately calculated as $I_{\mathrm{noise}} = V_{\mathrm{filter}}/(Z_{L\mathrm{cm}} + Z_{\mathrm{LISN}})$. The study in [1]–[3], and [4] states that the parasitics of the filter can increase $Z_{\mathrm{C}y}$ or reduce $Z_{L\mathrm{cm}}$, which result in the increasing of I_{noise}. According to the definition of V_{filter}, it is also obvious that the decreasing of Z_{source} will also increase V_{filter} and further increase the noise

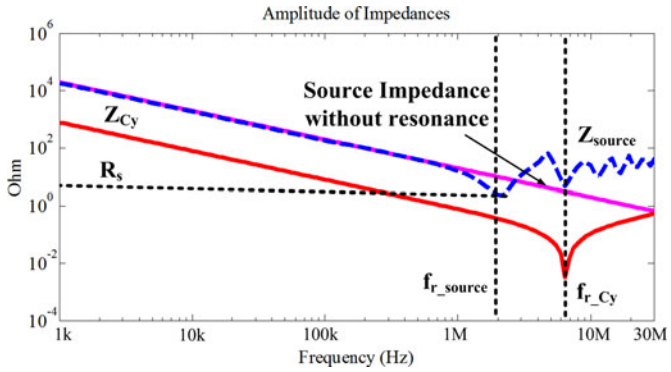

Fig. 5. Small-signal impedances of C_y capacitor and ac side noise propagation path.

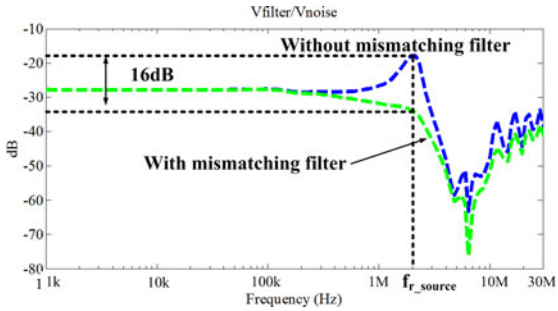

Fig. 6. Ratios between $V_{\rm filter}$ and $V_{\rm noise}$.

current. Therefore, the filter's high-frequency attenuation can be estimated by comparing these impedances.

Fig. 5 illustrates the plots of different impedances. The pink curve shows the estimated ac side source impedance without resonance, which is the impedance of the grounding capacitance. $Z_{\rm source}$ in blue is the measured impedance of ac side cable and motor. $Z_{\rm source}$ has a resonant peak at 2 MHz ($f_{r\_{\rm source}}$), which is corresponding to the resonant frequency of the main parasitic inductance and the stray capacitance of the ac side cable and load. Above 2 MHz, the transmission-line effect starts taking place and contributes multiple resonances at high frequencies. Z_{Cy} is the impedance of C_y capacitors on the dc side, which is a typical capacitor with its equivalent-series inductance (ESL).

As shown in Fig. 5, the resonance at the frequency $f_{r\_{\rm source}}$ makes $Z_{\rm source}$ (blue) much lower than the impedance without resonance (pink). According to aforementioned analysis, the decreasing of $Z_{\rm source}$ leads to the increasing of $V_{\rm filter}$ as the blue plot shown in Fig. 6, and it sequentially causes the increasing of noise current. Fig. 6 illustrates the noise voltage attenuation $V_{\rm filter}/V_{\rm noise}$. At low frequencies, $V_{\rm noise}$ can be effectively attenuated by -28 dB. This attenuation curve starts rising at 1 MHz, and increases from -28 to -18 dB at 2 MHz, which is corresponding to the resonance of $Z_{\rm source}$. It is notable that the degradation exists at $f_{r\_{\rm source}} < f_{r\_Cy}$, where the C_y capacitor has not hit its parasitic effect yet. The resonance of the noise source impedances can degrade the filter's in-circuit performance even the parasitics of the filter have not shown their impacts yet. Regardless $Z_{\rm source} > Z_{Cy}$ or $Z_{\rm source} < Z_{Cy}$, as long as $f_{r\_{\rm source}} < f_{r\_Cy}$ and $Z_{\rm source}$ decreases, $V_{\rm filter}$ increases and so does the noise current. In cases that $f_{r\_{\rm source}} >= f_{r\_Cy}$,

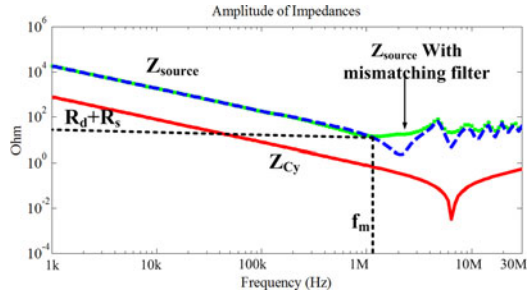

Fig. 7. Small-signal impedances comparisons with mismatching filter.

both Z_{Cy} and $Z_{\rm source}$ will change, and the attenuation depends on the ratios between these impedances.

IV. Design of the Impedance-Mismatching Filter and Its Experimental Validation

As stated in the last section, the resonance in the $Z_{\rm source}$ creates low CM impedances and results in the CM noise current spike. Lei and Jian [15] have proposed different optimal filter damping designs for the consideration of stability. Similarly, adding a proper damping branch will increase $Z_{\rm source}$ and reduce the noise current at the resonant frequency. Thus, the damping branch is also called "impedance-mismatching filter." This impedance-mismatching filter can be placed either on the ac side or on the dc side since the CM propagation paths on both sides are highly coupled [9]. According to Lei and Jian [15], an *RC*-parallel damping branch does not fit in the case in this letter since the total CM capacitance is limited by safety standards [12]. An *RL*-parallel damping branch is also not suitable for this application since the inductance which needs damping is from the parastics. Therefore, the *RL*-series damping has been chosen for tailoring the $Z_{\rm source}$. Then the problem is simplified to be "an *RL*-series damping for an *LC* filter." The design procedure of the mismatching filter can be concluded as following steps:

Step1: Measure the ac-side CM offline impedance of the using impedance analyzer, this measurement configuration can be illustrated as shown in Fig. 4. The impedance information can be read on the data file from the impedance analyzer as illustrated in Fig. 5. The stray capacitance C_s and the parasitic inductance L_s at low frequencies can be estimated by curve fitting using Fig. 5. Regarding the case in this letter, $C_s = 5$ nF, $L_s = 1.2\ \mu$H, $C_y = 200$ nF, $f_0 = f_{r\_{\rm source}} = 2$ MHz, and $R_s = 2.5\ \Omega$. Define R_s as the resistive part of the ac side cable and load, which is in series with L_s and R_s.

Step 2: Based on curve-fitting results, calculate the characteristic impedance$||Z_0|| = \sqrt{L_s/C_s} = 1/2\pi f_0 C_s = 16\ \Omega$. Since the $Z_{\rm source}$ shows a typical characteristic of an RLC series circuit, we can define its damping factor: $\zeta = (R_s + R_d)/||Z_0||$. In this definition, $\zeta > 1$ is overdamped, $\zeta < 1$ is underdamped, while $\zeta = 1$ is the critical damped condition. To damp the resonance in $Z_{\rm source}$, we should have $R_s + R_d >= ||Z_0||$. Generally, R_d can be calculated using (1). Since R_s in this letter is much smaller than $||Z_0||$,we can simply make $R_d = ||Z_0|| = 16\ \Omega$ to make the system slightly overdamped, $\zeta =$

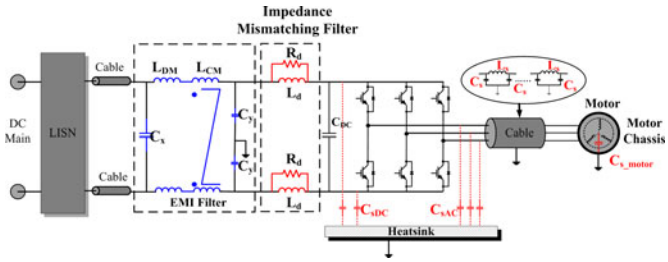

Fig. 8. Installation of the impedance-mismatching filter.

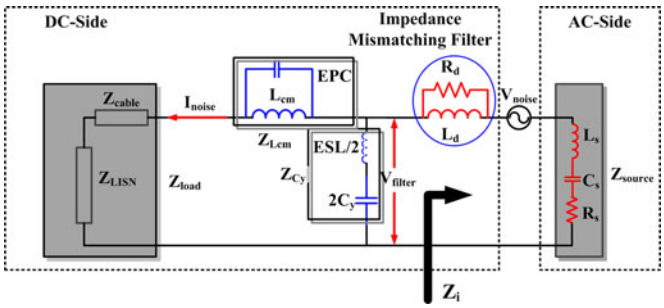

Fig. 9. CM equivalent circuit with the impedance-mismatching filter.

$$(R_d + R_s)/||Z_0|| = 1.16$$

$$R_d = \zeta||Z_0|| - R_s = \zeta\sqrt{L_s/C_s} - R_s = \zeta/2\pi f_0 C_s - R_s \tag{1}$$

where $\zeta >= 1$.

Step 3: Choice of L_d. Define f_m to be the roll-over frequency of the damping branch, below $f_m, Z_{Ld} < R_d, L_d$ provides the low impedance path for low-frequency currents, at frequencies above $f_m, Z_{Ld} > R_d, Z_{Ld} = 2\pi f_m L_d > R_d$, the noise current will be bypassed by R_d, and the total impedance is resistive until L_s contributes again. To have a smooth attenuation, we choose $Z_{Cs} = Z_{Ld} = R_d + Rs = \zeta||Z_0||$, where $Z_{Cs} = 1/(2\pi f_m C_s), Z_{Ld} = 2\pi f_m L_d$, so that f_m and L_d can be calculated as (2) and (3). Substituting the parameters in this letter into (1)–(3), we will have $R_d = 16\ \Omega$, $f_m = 1.7$ MHz, $L_d = 1.7\ \mu$H

$$f_m = \frac{1}{2\pi\left(R_d + R_s\right)C_s} = \frac{1}{2\pi\zeta||Z_0||C_s} \tag{2}$$

$$L_d = \frac{\left(R_d + R_s\right)}{2\pi f_m} = \frac{\zeta||Z_0||}{2\pi f_m}. \tag{3}$$

Following the proposed steps, an impedance-mismatching filter has been designed for this motor drive system. The installation of this filter is between the main *LC* EMI filter and the dc capacitor as shown in Figs. 8 and 9 illustrates its CM equivalent circuit. In this letter, the damping branch is placed on the dc side of the motor drive since it requires less winding and potentially has smaller size, however, it modifies the ac side CM impedance seeing from the EMI filter (Z_i), as shown in Fig. 9. The impedance-mismatching filter is much smaller than the EMI filter which takes care of the noises for the whole testing range. Thus, the impedance-mismatching filter can be considered as a "baby filter" of the "main filter." With inserting the mismatching filter between the main filter and the converter, the impedance of

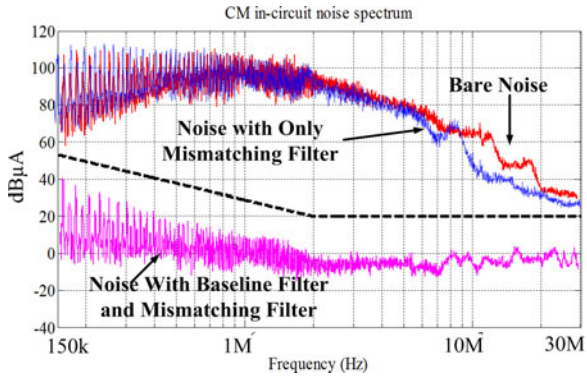

Fig. 10. Noise spectrum with the baseline filter and the impedance-mismatching filter.

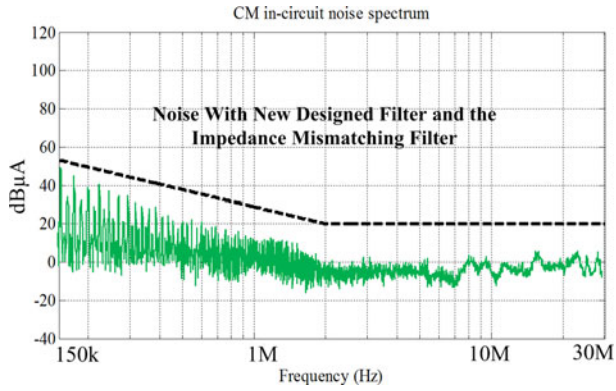

Fig. 11. Noise spectrum with the improved filter and the impedance-mismatching filter.

the noise source seeing from the filter side has been modified as shown in Fig. 7. The green curve illustrates the impedance with the mismatching filter. At the 2 MHz point, the impedance of the green curve is much higher than the blue curve. It is also can be seen in Fig. 6 that the attenuation at f_{r_source} gains -16 dB with the impedance-mismatching filter. With the impedance-mismatching filter, the pink noise spectrum in Fig. 10 shows that the spike at 2 MHz has been attenuated. The blue spectrum in Fig. 10 shows the noise with only the damping branch. The damping inductor is very small and the noise current will not be suppressed much if only this part is installed. It only attenuates some noises above 10 MHz. According to the result in Fig. 10, the noise spectrum is overattenuated. Hence, the main filter can be redesigned and potentially shrunk. With the mismatching filter, the main filter can be redesigned following the same rule provided by Maillet *et al.* [1], and the L_{cm} can be reduced to 450 μH. Fig. 11 shows the noise spectrum with this improved main filter and impedance-mismatching filter. Although the CM inductance of the improved filter is only 0.15 times of the baseline filter, it still provides enough attention for whole EMI testing range. The reduction of the CM inductor is shown in Fig. 12. This experiment proves that the multistage "main filter + baby filter" structure gives good attenuation with small size and volume of the filter. The CM choke in the baseline filter uses four J-ferrite toroid cores (ZJ44916TC, Diameter 49 mm, Height, 15.6 mm) and 11 turns while the CM choke in the improved filter uses only one core. The damping inductor is implemented

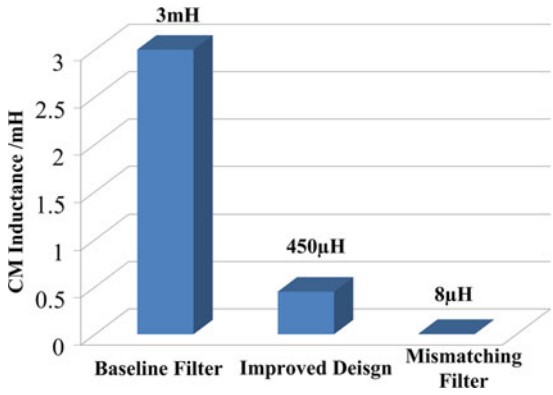

Fig. 12. Comparison of the CM inductances.

by two separated MPP toroid cores (C055266A2, diameter 6.6 mm, height: 4.8 mm). Since the value of L_d is small, using or not using couple inductor in a discrete filter would not show too much difference in the size. L_d is rather small compared to the DM inductors, thus, adding this impedance-mismatching filter will not influence the voltage ripple on the dc-link capacitor. Besides, the reduction on the inductors gives more opportunity for the filter integration to achieve higher power density [7], [11].

Moreover, based on the analyses and experiment above, properly damping of the noise propagation path resonances using the impedance-mismatching filter can efficiently improve the main filter's performance, and the main filter's performance accommodates with its low frequency design even at high frequencies. Therefore, an improved EMI filter design procedure can be proposed as following steps:

1) measure/estimate the noise propagation path impedances; measure the bare noise;
2) observe the impedances and determine the resonance of the impedance of the noise propagation path;
3) determine the critical resonance, damp these resonances using the approaches stated at the beginning of this section, design the impedance-mismatching filter, in the case that multiply resonances needs to be damped, R_d should be chosen to cover the one requires most damping impedance;
4) design the main filter using the procedure proposed in [1].

V. Discussions of the Impacts from Parasitics

According to the analysis in the previous sections, adding an *RL*-series damping branch can help to improve the filter's high-frequency performance. However, the parasitics from different components could bring unexpected influences. The EPC of the CM inductor decreases the inductor impedance at high frequencies, but this impedance is still much higher than $Z_{\rm source}$ and Z_{Cy}, thus, the EPC of CM inductor will not influence much on the damping. ESL of the C_y capacitor determines the resonance frequency of Z_{Cy}, thus, the EPC across the damping inductor L_d could hurt the inductor's high-frequency impedance. However, L_d is small, so that only several turns are needed for its winding. Therefore, EPC of L_d can be very small too, and the resonant frequency of L_d can be much higher than the frequency where the damping is needed. Loss on the damping resistor R_d is another issue. In this case, the converter switches at 12 kHz, the energy of its noise current at 2 MHz is low, therefore, the loss on R_d is not a main concern.

VI. Conclusion

This letter investigates into a cause which degrades the high-frequency performance of an *LC* CM EMI filter. It proves that the resonance in the noise propagation path results in unexpected noise spikes and leads to massive overdesign of the filter. This letter proposes to use a small impedance-mismatching filter to damp the resonance in the propagation path. This multistage "main filter + baby filter" structure gives good attenuation with small size and volume of the filter. A modified design procedure for EMI filters with this "impedance-tailoring" technique is also proposed in this letter. The proposed method is "impedance sensitive" and requires offline measurement each time. Once the system setup is fixed, its impedances will be fixed too; the design of the filter will need to be "tailored" according to the specific motor/cable/converter configuration.

References

[1] Y. Maillet, L. Rixin, W. Shuo, W. Fei, R. Burgos, and D. Boroyevich, "High-density EMI filter design for DC-fed motor drives," *IEEE Trans. Power Electron.*, vol. 25, no. 5, pp. 1163–1172, May 2010.
[2] W. Shuo, F. C. Lee, and J. D. Van Wyk, "Inductor winding capacitance cancellation using mutual capacitance concept for noise reduction application," *IEEE Trans. Electromagn. Compat.*, vol. 48, no. 2, pp. 311–318, May 2006.
[3] W. Shuo, F. C. Lee, and W. G. Odendaal, "Cancellation of capacitor parasitic parameters for noise reduction application," *IEEE Trans. Power Electron.*, vol. 21, no. 4, pp. 1125–1132, Jul. 2006.
[4] W. Shuo, F. C. Lee, D. Y. Chen, and W. G. Odendaal, "Effects of parasitic parameters on EMI filter performance," *IEEE Trans. Power Electron.*, vol. 19, no. 3, pp. 869–877, May 2004.
[5] H. Hui-fen and D. Liang-Yong, "Improving the high-frequency performance of integrated EMI filter with multiple ground layers," in *Proc. Asia-Pacific Symp. Electromagn. Compat.*, 2012, pp. 249–252.
[6] W. Shuo, Y. Y. Maillet, F. Wang, L. Rixin, R. Burgos, and L. Fang, "Investigating the grounding of EMI filters in power electronics systems," in *Proc. IEEE Power Electron. Spec. Conf.*, 2008, pp. 1625–1631.
[7] L. Fang, A. C. Baisden, D. Boroyevich, K. D. T. Ngo, W. Shuo, and P. Mattavelli, "Design of a hybrid busbar filter combining a transmission-line busbar filter and a one-turn inductor for DC-fed three-phase motor drive systems," *IEEE Trans. Power Electron.*, vol. 28, no. 12, pp. 5588–5602, Dec. 2013.
[8] L. Fang, D. Boroyevich, and P. Mattavelli, "Improving EMI filter design with in circuit impedance mismatching," in *Proc. IEEE 27th Annu. Appl. Power Electron. Conf. Expo.*, 2012, pp. 1652–1658.
[9] L. Fang, Z. Xuning, D. Boroyevich, P. Mattevelli, X. Jing, F. Wang, and N. Gazel, "On discussion of AC and DC side EMI filters design for conducted noise suppression in DC-fed three phase motor drive system," in *Proc. IEEE 26th Annu. Appl. Power Electron. Conf. Expo.*, 2011, pp. 667–672.
[10] RTCA, "RTCA/DO-160E," 2004.
[11] L. Fang, R. Robutel, W. Shuo, F. Wang, and D. Boroyevich, "Integrated input EMI filter for a 2 kW DC-fed 3-phase motor drive," in *Proc. IEEE 24th Annu. Appl. Power Electron. Conf. Expo.*, 2009, pp. 325–329.
[12] U. S. Department of Defense Interference Standard, "MIL-461-F," 2007.
[13] L. Fang, W Shuo, W. Fei, D. Boroyevich, N. Gazel, K. Yong, and A. C. Baisden, "Analysis of CM volt-second influence on CM inductor saturation and design for input EMI filters in three-phase DC-fed motor drive systems," *IEEE Trans. Power Electron.*, vol. 25, no. 7, pp. 1905–1914, Jul. 2010.
[14] X. Lei and S. Jian, "Conducted common-mode EMI reduction by impedance balancing," *IEEE Trans. Power Electron.*, vol. 27, no. 7, pp. 1084–1089, Jul. 2012.
[15] X. Lei and S. Jian, "Optimal damping of multistage EMI filters," *IEEE Trans. Power Electron.*, vol. 27, no. 3, pp. 1220–1227, Mar. 2012.